Dissipation of core-hole momentum by phonons in soft-x-ray radiation processes from valence band to core level of wide-gap insulators

Tatsuya Minami and Keiichiro Nasu
Photon Factory, National Laboratory for High Energy Physics, The Graduate University for Advanced Studies, 1-1, Oho, Tsukuba, Ibaraki 305, Japan
(Received 4 February 1997)

The role of phonons in the soft-x-ray radiation process from a valence band to a core level in an insulator is studied theoretically. A three-band system composed of a dispersionless core band, a conduction band, and a valence band, with wide energy gaps between them, is taken as a typical example. Phonons with a finite dispersion are assumed to couple weakly only with a hole in the core band (core hole). Using this model, we calculate the resonant second-order optical process composed of an excitation of an electron from the core band to the conduction band by an incident x ray, and a subsequent transition from the valence band to the core band by radiating another x ray. Without the phonons, the momentum of the core hole is expected to be well defined by the resonance condition of the incident x ray. However, this momentum is dissipated by the phonons. If the radiation occurs completely after this dissipation, we obtain a so-called luminescence, which is independent of the incident x ray. In this case, the spectral shape fully reflects the density of states (DOS) of the valence band. However, if the radiation occurs long before this dissipation effect, we obtain a resonant Raman scattering that depends on the incident x ray. The spectral shape of this Raman scattering has a sharp peak, quite different from the DOS. The relative intensity between these two components is determined by the phonon dispersion, the lifetime of the core hole, and the core-hole–phonon coupling constant. From this theoretical framework, we have concluded that there are various cases, i.e., Raman-dominant cases and luminescence-dominant cases, as well as intermediate cases, in good agreement with various experimental observations. The B $1s \leftrightarrow 2p$ transitions of cubic BN are concluded to correspond to a luminescence-dominant case. [S0163-1829(98)02619-8]

I. INTRODUCTION

In the research field of soft-x-ray spectroscopy for solids, one of the most important problems is how to determine the density of states (DOS) of the valence band of each solid correctly. The standard method to obtain information about this DOS is photoemission spectroscopy (PES). In this method, as is well known, a valence electron in a solid is emitted toward the outside of the solid after the excitation by an incident x ray. Analyzing the kinetic energy of this emitted electron, we can finally determine the aforementioned DOS. Thus this method has already greatly contributed to the development of solid-state physics, and this situation will not be changed even in the future. However, PES has some weaknesses, since the probe in this method is the emitted electron itself. It must go through the surface of a solid before it is detected, and, in some cases, the kinetic motion of this electron may be disturbed by this surface. Surfaces differ from one another, and hence the information of the DOS will be blurred. Moreover, the whole experimental apparatus of this method must be kept in an ultrahigh vacuum to prevent the electron from being scattered by the atmosphere.

Recently, the soft-x-ray radiation spectroscopy (SXRS) was proposed as an alternative method to determine the DOS. This method is mostly free from the aforementioned weaknesses, because its probe is the soft x ray radiated from a solid. Figure 1 schematically shows a set of optical processes relevant to this SXRS. This is a resonant second-order optical process, different form previous PES, which is a first-order optical process. At the first step of the SXRS, as shown in Fig. 1, an electron is resonantly excited from a core band to a conduction band by an incident soft x ray. Thus we obtain a conduction electron and a vacancy (core hole) in the core band which has no energy dispersion. At the second step, a valence electron, as well as an excited electron in the conduction band, can go down to the core band by radiating a secondary soft x ray. Throughout this paper, as shown in Fig. 1, we focus only on the transition process from the valence band to the core band, as well as on the aforemen-

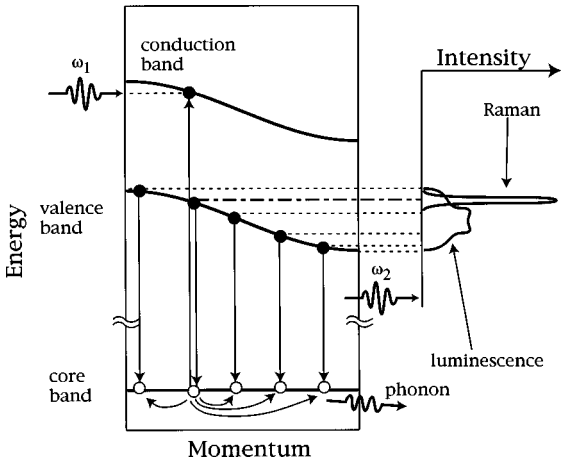

FIG. 1. Schematic three-band system and the resonant second-order optical process (left portion). The spectrum of the x-ray radiation (right portion).

tioned excitation process. Analyzing the energy distribution of the radiated x ray, we obtain information about the DOS. Generally speaking, this type of experimental measurement is very difficult, because the intensity of the second-order radiation is usually very weak. Nevertheless, this difficulty is removed gradually as the brilliance of the synchrotron radiation increases. At present, SXRS is becoming more and more popular day by day.

Various experimental results have already been reported by using the SXRS method. In these observed spectra, we can clearly see two typical but rather different components. One is a component whose peak in the spectra shifts as the incident x-ray energy changes. We call this the Raman component according to the conventional terminology for the optics in the visible region. Another is a component whose spectral shape does not change, even if the incident energy is changed. We call this the luminescence. Intensity ratios between these two components change from solid to solid. In the case of the B $1s \leftrightarrow 2p$ transitions of cubic BN reported by Agui *et al.*, [1] and in the case of hexagonal BN reported by Jia *et al.*, [2] the luminescence is dominant, and the resonance Raman component is very weak. Both components are comparable, in the case of the Ti $2p \leftrightarrow 3d$ transitions of TiO_2 reported by Tezuka *et al.*, [3] and also in the case of the Ca $2p \leftrightarrow 3d$ transitions of CaSi and $CaSi_2$ reported by Jia *et al.* [4] On the other hand, in the case of the Mn $2p \leftrightarrow 3d$ transitions of MnO reported by Butorin *et al.*, [5] the Raman component is dominant and the luminescence component cannot be seen.

If we return to the case of cubic BN, an effect of the coupling between the core hole and phonons is also clearly observed in the light absorption spectrum of the B $1s \rightarrow 2p$ excitation region. [6] This coupling is expected to play a very important role to make the luminescence dominant in this case. There are many other cases [7] wherein the core-hole–phonon coupling is very important in the soft-x-ray spectroscopy.

In the present stage of theoretical studies for the SXRS, however, there is no systematic method to clarify why the whole spectral shape separates into Raman component and luminescence component. It is also unknown how the information about the DOS is included in the spectral shape. The purpose of the present paper is to clarify these points theoretically. For this purpose, we will take a typical three-band system in an insulator. It is composed of a dispersionless core band, a conduction band, and a valence band, with wide energy gaps between them. Phonons with a finite dispersion are assumed to couple weakly with only the core hole created by the incident x ray. Using this model, we will calculate the resonant second-order optical process, composed of an excitation of an electron from the core band to the conduction band by the incident soft x ray, and a subsequent transition from the valence band to the core band caused by radiating another soft x ray. When the energy of the incident x ray is given, the momentum of the core hole is well defined by the resonance condition, as easily seen from Fig. 1. However, its momentum is dissipated by the interaction with the phonons. The time required for this dissipation (dissipation time) is determined only by the dispersion of the phonon energy, because the core band has no energy dispersion. If the x-ray radiation occurs after this dissipation is completed, we obtain the luminescence, as schematically shown in Fig. 1. In this case, the spectral shape fully reflects the DOS, being independent of the incident energy, while, if the radiation occurs long before this dissipation effect, we obtain the Raman component. In this case, the spectral shape has a sharp peak, being much different from the DOS, and depends on the incident energy. The relative intensity between these two components is determined by three factors: the dissipation time, the strength of the core-hole–phonon coupling, and the lifetime of the core hole itself. From this theoretical framework, we will show that there are various cases, i.e., Raman-dominant cases, luminescence dominant cases, and intermediate cases, in good agreements with various observed cases by recent experiments. The B $1s \leftrightarrow 2p$ transitions of cubic BN is concluded to correspond the luminescence-dominant case. In Sec. II, we will present our model Hamiltonian.

II. MODEL HAMILTONIAN

Let us consider a model composed of an electronic system interacting with photons and phonons. The total Hamiltonian H of our system is written as

$$H \equiv H_e + H_p + H_L + H_{eL} + H_{\rm ep}, \tag{2.1}$$

where H_e denotes the Hamiltonian of the electronic system based on the tight-binding picture, and is composed of an electron and holes. H_e is given as

$$H_e \equiv \varepsilon_c \sum_l c_l^\dagger c_l + \left(\frac{\varepsilon_g}{2} + 6T_v \right) \sum_l v_l^\dagger v_l - T_v \sum_{\langle l,l' \rangle} v_{l'}^\dagger v_l + \left(\frac{\varepsilon_g}{2} + 6T_a \right) \sum_l a_l^\dagger a_l \pm T_a \sum_{\langle l,l' \rangle} a_{l'}^\dagger a_l, \tag{2.2}$$

where $c_l^\dagger$, $v_l^\dagger$, and $a_l^\dagger$ are creation operators of a core hole, a valence hole, and a conduction electron, respectively, in a lattice site specified by a position vector l. The lattice structure is taken to be a simple cubic. The unit of length is the lattice constant. ε_c (>0) is an energy of the core hole, which is usually of the order of 100 eV. ε_g (>0) is the energy gap between the conduction and valence bands. All the one-body energies are referenced from the center of this energy gap. T_v (>0) and T_a (>0) denote the intersite transfer energies of the valence hole and the conduction electron, respectively, which are assumed not to be zero only between the neighboring two lattice sites l and l'. The symbol $\Sigma_{\langle l,l' \rangle}$ denotes this conditional summation over l and l'. When the sign of the last term of Eq. (2.2) is $+$, the energy gap becomes indirect, while the minus sign corresponds to a direct gap. This notation will be used hereafter. In this paper we treat a solid whose conduction- and valence-band-widths are wide enough, that is, T_v and T_a are of the order of 1 eV. For simplicity, all holes and electrons are assumed to be spinless. Throughout this paper, we also neglect the Coulombic interactions between the electrons and the holes.

In Eq. (2.1), H_p denotes the Hamiltonian of photon, and is given as

$$H_p \equiv \sum_k \omega_k b_k^\dagger b_k, \tag{2.3}$$

where $b_k^\dagger$ is the creation operator of a photon with a wave vector k and an energy ω_k ($\hbar=1$). Throughout this paper, we also omit the polarization of the photon for simplicity. The symbol H_L denotes the Hamiltonian of the phonon, and is given as

$$H_L \equiv \sum_q \Omega_q B_q^\dagger B_q , \tag{2.4}$$

where $B_q^\dagger$ is the creation operator of a phonon with a wave vector q and an energy Ω_q. As a typical example of phonon dispersion, we take an optical phonon with a central energy Ω and with a width 6γ. In this case, Ω_q is given as

$$\Omega_q = \Omega + \gamma[\cos(q_x)+\cos(q_y)+\cos(q_z)], \tag{2.5}$$

where q_x, q_y, and q_z denote the Cartesian components of q. In the cases of various solids referenced in Sec. I, Ω_q is about 0.2 eV or less. This energy is negligibly small compared with ε_c, while its wave vector q can take various values in the first Brillouin zone of this simple cubic lattice, and will play an important role.

In Eq. (2.1), H_{eL} denotes the linear coupling between the core hole and the phonon, and is given as

$$H_{eL} \equiv -N^{-1/2}\sum_{l,q} \Omega_q S_q^{1/2} e^{-iq\cdot l} c_l^\dagger c_l (B_q^\dagger + B_{-q}), \tag{2.6}$$

where S_q is a dimensionless coupling constant between the core hole and the phonon. N denotes the total number of lattice sites in the solid. Here we should note that $(6\gamma)^{-1}$ is the dissipation time of the phonon.[8] It is a time within which localized wave packets of phonons generated through H_{eL} around at a certain site, propagate and dissipate all over the solid.

In the present paper, we treat only the case where hole- (or electron-) phonon couplings are weak, that is, $N^{-1}\Sigma_q S_q \simeq 1$. In this weak case, according to Migdal's theorem, the effects of coupling on the conduction electron and valence hole are very small, since they have wide energy bands. In the case of the core hole, however, even if this interaction is weak, it becomes very important because the core hole has no bandwidth. From this point of view, we have neglected the couplings of phonons with the conduction electron and valence hole.

In Eq. (2.1), $H_{\rm ep}$ denotes the electron-photon interaction, and is given as

$$H_{ep} \equiv N^{-1/2}\sum_{k,l} (b_k e^{-ik\cdot l} + b_k^\dagger e^{ik\cdot l})\{[M_{ac}(k) a_l^\dagger c_l^\dagger + M_{vc}(k) c_l v_l^\dagger] + \text{H.c.}\}. \tag{2.7}$$

$M_{ac}(k)$ and $M_{vc}(k)$ are the transition dipole matrix elements between the core and conduction bands, and between the valence and the core bands, respectively.

Let us now denote the state of the electron-photon system by $|x\rangle\rangle$, which is a direct product of the photon part $|n_{k_1}, n_{k_2}\rangle$ and the electronic part $|\varphi)$ as

$$|x\rangle\rangle = |n_{k_1}, n_{k_2}\rangle |\varphi), \tag{2.8}$$

wherein the photon part is denoted by the number representation. n_{k_1} is the number of the incident photon with a wave vector k_1 and an energy ω_1. n_{k_2} denotes a number of the radiated photon with a wave vector k_2 and an energy ω_2. The lowest state of the electronic part is the electron-hole vacuum. We denote it by $|0)$, and its energy is zero. The excited state $|\phi_{lk})$ with a core hole and a conduction electron is defined as

$$|\phi_{lk}) \equiv a_k^\dagger c_l^\dagger |0), \quad a_k^\dagger \equiv N^{-1/2}\sum_l e^{-ik\cdot l} a_l^\dagger , \tag{2.9}$$

where $a_k^\dagger$ is the Fourier transform of $a_l^\dagger$ with a wave vector k. Thus the conduction electron with a wave vector k is defined, and its energy $\varepsilon_a(k)$ is given as

$$\varepsilon_a(k) \equiv \left(\frac{\varepsilon_g}{2} + 6T_a\right) \pm 2T_a[\cos(k_x) + \cos(k_y) + \cos(k_z)]. \tag{2.10}$$

The excited state $|\psi_{Kk})$, which has a valence hole and a conduction electron with a total wave vector K, is defined as

$$|\psi_{Kk}) \equiv a_k^\dagger v_{K-k}^\dagger |0), \quad v_k^\dagger \equiv N^{-1/2}\sum_l e^{-ik\cdot l} v_l^\dagger . \tag{2.11}$$

Here $v_k^\dagger$ is the Fourier transform of $v_l^\dagger$ with a wave vector k. Thus the valence hole with a wave vector k is also defined, and its energy $\varepsilon_v(k)$ is given as

$$\varepsilon_v(k) \equiv \left(\frac{\varepsilon_g}{2} + 6T_v\right) - 2T_v[\cos(k_x) + \cos(k_y) + \cos(k_z)]. \tag{2.12}$$

To make the latter formulation convenient, we now define the effective Hamiltonian of the core-hole–phonon coupled system. We can write the effective Hamiltonian (H_g) of the phonon without the core hole as

$$H_g = H_L . \tag{2.13}$$

The effective Hamiltonian ($H_{\rm exl}$) of the phonon, with a core hole at site l, is given as

$$H_{\rm exl} = H_L - N^{-1/2}\sum_q \Omega_q S_q^{1/2} e^{-iq\cdot l}(B_q^\dagger + B_{-q}). \tag{2.14}$$

In Sec. III, we will calculate the transition rate of the aforementioned resonant second-order optical process.

III. TRANSITION RATE OF THE RESONANT SECOND-ORDER OPTICAL PROCESS

We denote the initial state of the electron-photon system by $|i\rangle\rangle$, and its energy by E_i. Using the notation introduced in Eq. (2.8), we can rewrite it as

$$|i\rangle\rangle = |1,0\rangle |0)). \tag{3.1}$$

Meanwhile, we denote the intermediate state and its energy by $|m\rangle\rangle$ and E_m. This state $|m\rangle\rangle$ is rewritten as

$$|m\rangle\rangle = |0,0\rangle |\phi_{lk}). \tag{3.2}$$

Similarly, we denote the final state and its energy by $|f\rangle\rangle$ and E_f. This state $|f\rangle\rangle$ is rewritten as

$$|f\rangle\rangle = |0,1\rangle|\psi_{Kk}). \tag{3.3}$$

Using these notations, we can now define the density matrix ρ_0 of the initial state of the total system at time $t=0$ as

$$\rho_0 \equiv |i\rangle\rangle \frac{e^{-\beta H_g}}{\mathrm{Tr}[e^{-\beta H_g}]} \langle\langle i|, \tag{3.4}$$

where $\beta \equiv 1/(k_B T)$, k_B is Boltzmann's constant, and T is the temperature. The symbol Tr denotes the trace with respect to phonons. The time evolution of the density matrix $\rho(t)$ at time t, started from this initial state, can be formally denoted as

$$\rho(t) \equiv e^{-iHt} \rho_0 e^{iHt}. \tag{3.5}$$

The transition probability $P(\omega_1, \omega_2, t)$ from the initial state to the final state at time t is given as

$$P(\omega_1, \omega_2, t) \equiv \mathrm{Tr}\left[\sum_f \langle\langle f|\rho(t)|f\rangle\rangle \right]. \tag{3.6}$$

Expanding e^{-iHt} and e^{iHt} with respect to H_{ep} up to second order, we obtain

$$\begin{aligned} P(\omega_1, \omega_2, t) = & \int_0^t dt_1 \int_0^{t_1} dt_2 \int_0^t dt_1' \int_0^{t_1'} dt_2' \\ & \times \mathrm{Tr}\left[\sum_f \langle\langle f|H_{\mathrm{ep}}(t_1) H_{\mathrm{ep}}(t_2) \rho_0 \right. \\ & \left. \times H_{\mathrm{ep}}(t_2') H_{\mathrm{ep}}(t_1')|f\rangle\rangle \right], \end{aligned} \tag{3.7}$$

where

$$H_{\mathrm{ep}}(t) \equiv e^{iH't} H_{\mathrm{ep}} e^{-iH't}, \quad H' \equiv H_e + H_p + H_L + H_{eL}. \tag{3.8}$$

Using Eqs. (2.13), (2.14), (3.1), and (3.2), we can rewrite Eq. (3.7) as

$$\begin{aligned} P(\omega_1, \omega_2, t) = & \sum_f \sum_{m,m'} \langle\langle f|H_{\mathrm{ep}}|m\rangle\rangle \langle\langle m|H_{\mathrm{ep}}|i\rangle\rangle \\ & \times \langle\langle i|H_{\mathrm{ep}}|m'\rangle\rangle \langle\langle m'|H_{\mathrm{ep}}|f\rangle\rangle \\ & \times \int_0^t dt_1 \int_0^{t_1} dt_2 \int_0^t dt_1' \int_0^{t_1'} dt_2' \\ & \times e^{iE_f(t_1 - t_1') + iE_m(t_2 - t_1) - iE_{m'}(t_2' - t_1') - iE_i(t_2 - t_2')} \\ & \times \langle e^{-iH_{\mathrm{exl}'}(t_2' - t_1')} e^{iH_g(t_1 - t_1')} e^{iH_{\mathrm{exl}}(t_2 - t_1)} \\ & \times e^{-iH_g(t_2 - t_2')} \rangle. \end{aligned} \tag{3.9}$$

Here l and l' denote sites in which the core hole is generated, and the symbol $\langle \cdots \rangle$ denotes the average with respect to H_g,

$$\langle \cdots \rangle \equiv \frac{\mathrm{Tr}[\cdots e^{-\beta H_g}]}{\mathrm{Tr}[e^{-\beta H_g}]}. \tag{3.10}$$

Changing the set of time variables from (t_1, t_2, t_1', t_2') to (x, σ, τ, τ') as

$$x \equiv \frac{t_1 + t_1'}{2}, \quad \sigma \equiv t_1 - t_1', \quad \tau \equiv t_2 - t_1, \quad \tau' \equiv t_2' - t_1', \tag{3.11}$$

we can rewrite $P(\omega_1, \omega_2, t)$ for large t, as

$$\begin{aligned} P(\omega_1, \omega_2, t) = & \sum_f \sum_{m,m'} \langle\langle f|H_{\mathrm{ep}}|m\rangle\rangle \langle\langle m|H_{\mathrm{ep}}|i\rangle\rangle \\ & \times \langle\langle i|H_{\mathrm{ep}}|m'\rangle\rangle \langle\langle m'|H_{\mathrm{ep}}|f\rangle\rangle \\ & \times t \int_{-t}^t d\sigma \int_0^t d\tau \int_0^t d\tau' \\ & \times e^{i(E_f - E_i)\sigma + i(E_m - E_i)\tau - i(E_{m'} - E_i)\tau'} \\ & \times \langle e^{iH_g \tau'} e^{-iH_{\mathrm{exl}'}\tau'} e^{iH_g \sigma} e^{iH_{\mathrm{exl}}\tau} e^{-iH_g \tau} e^{-iH_g \sigma} \rangle. \end{aligned} \tag{3.12}$$

It is well known that the transition rate $R(\omega_1, \omega_2)$ is defined by the relation

$$R(\omega_1, \omega_2) \equiv \left. \frac{\partial P(\omega_1, \omega_2, t)}{\partial t} \right|_{t \to \infty}, \tag{3.13}$$

and substituting Eq. (3.12) into its right-hand side, we obtain

$$\begin{aligned} R(\omega_1, \omega_2) = & \sum_f \sum_{m,m'} \langle\langle f|H_{\mathrm{ep}}|m\rangle\rangle \langle\langle m|H_{\mathrm{ep}}|i\rangle\rangle \langle\langle i|H_{\mathrm{ep}}|m'\rangle\rangle \\ & \times \langle\langle m'|H_{\mathrm{ep}}|f\rangle\rangle \int_{-\infty}^{\infty} d\sigma \int_0^{\infty} d\tau \int_0^{\infty} d\tau' \\ & \times e^{i(E_f - E_i)\sigma + i(E_m - E_i)\tau - i(E_{m'} - E_i)\tau'} \\ & \times \langle e^{iH_g \tau'} e^{-iH_{\mathrm{exl}'}\tau'} e^{iH_g \sigma} e^{iH_{\mathrm{exl}}\tau} e^{-iH_g \tau} e^{-iH_g \sigma} \rangle. \end{aligned} \tag{3.14}$$

Now let us calculate the phonon part in Eq. (3.14). For this purpose, we use the following time-ordered exponential forms:

$$e^{iH_g \tau'} e^{-iH_{\mathrm{exl}'}\tau'} = T_+ \exp\left[-i \int_0^{\tau'} du' \Delta H_{l'}(u') \right], \tag{3.15}$$

$$e^{iH_g \sigma} e^{iH_{\mathrm{exl}}\tau} e^{-iH_g \tau} e^{-iH_g \sigma} = T_- \exp\left[i \int_0^{\tau} du \Delta H_l(u + \sigma) \right], \tag{3.16}$$

where $\Delta H_l(u)$ is defined as

$$\Delta H_l(u) \equiv e^{iH_g u} \Delta H_l e^{-iH_g u},$$

$$\Delta H_l \equiv -N^{-1/2} \sum_q \Omega_q S_q^{1/2} e^{-iq\cdot l}(B_q^\dagger + B_{-q}). \quad (3.17)$$

The symbols T_+ and T_- in Eqs. (3.15) and (3.16) denote positive and negative time orderings, respectively. From Eqs. (3.15) and (3.16), the phonon part in Eq. (3.14) is rewritten as

$$\langle e^{iH_g\tau'} e^{-iH_{\mathrm{exl}'}\tau'} e^{iH_g\sigma} e^{iH_{\mathrm{exl}}\tau} e^{-iH_g\tau} e^{-iH_g\sigma} \rangle = \left\langle T_+ \exp\left[-i \int_0^{\tau'} du' \Delta H_{l'}(u') \right] \times T_- \exp\left[i \int_0^{\tau} du \Delta H_l(u+\sigma) \right] \right\rangle. \quad (3.18)$$

For further calculation, we can use the cumulant expansion method. [9] Because the interaction is linear, we can terminate this cumulant expansion up to the second order, and obtain the following exact result:

$$\left\langle T_+ \exp\left[-i \int_0^{\tau'} du' \Delta H_{l'}(u') \right] T_- \exp\left[i \int_0^{\tau} du \Delta H_l(u+\sigma) \right] \right\rangle = \exp\left[-\int_0^{\tau'} du_1' \int_0^{u_1'} du_2' \langle \Delta H_{l'}(u_1') \Delta H_{l'}(u_2') \rangle \right] \exp\left[-\int_0^{\tau} du_1 \int_0^{u_1} du_2 \langle \Delta H_l(u_2) \Delta H_l(u_1) \rangle \right] \times \exp\left[\int_0^{\tau'} du' \int_0^{\tau} du \langle \Delta H_{l'}(u') \Delta H_l(u+\sigma) \rangle \right]. \quad (3.19)$$

Hereafter, we will be concerned only with the absolute zero temperature. Executing further calculations in each $\exp[\cdots]$ under this condition, we obtain

$$\left\langle T_+ \exp\left[-i \int_0^{\tau'} du' \Delta H_{l'}(u') \right] T_- \exp\left[i \int_0^{\tau} du\ \Delta H_l(u+\sigma) \right] \right\rangle = e^{-2S} e^{-iW(\tau-\tau')} \exp\left[N^{-1} \sum_q S_q e^{i\Omega_q \tau} \right] \exp\left[N^{-1} \sum_q S_q e^{-i\Omega_q \tau'} \right] \times \exp\left[N^{-1} \sum_q S_q e^{-iq\cdot(l-l')} e^{i\Omega_q \sigma} (e^{i\Omega_q \tau} - 1)(e^{-i\Omega_q \tau'} - 1) \right], \quad (3.20)$$

where S and W are the Huang-Rhys factor and the lattice relaxation energy, respectively, and they are defined as

$$S \equiv N^{-1} \sum_q S_q, \quad W \equiv N^{-1} \sum_q S_q \Omega_q. \quad (3.21)$$

So far, we have calculated the phonon part in Eq. (3.14), while we can also calculate the electron-photon part straightforwardly from Eqs. (2.9), (2.10), (2.11), (2.12), (3.1), (3.2), and (3.3). Consequently, we can obtain

$$R(\omega_1, \omega_2) = \frac{1}{N^3} |M_{vc}(k_2) M_{ac}(k_1)|^2 e^{-2S} \int_{-\infty}^{\infty} d\sigma \int_0^{\infty} d\tau \int_0^{\infty} d\tau' \sum_{K,k} \sum_{\Delta} e^{i(k_1 - k_2 - K)\cdot\Delta} \times e^{i[\varepsilon_a(k) + \varepsilon_v(K-k) + \omega_2 - \omega_1]\sigma + i[\varepsilon_a(k) + \varepsilon_c - W - \omega_1]\tau - i[\varepsilon_a(k) + \varepsilon_c - W - \omega_1]\tau'} \times \exp\left[N^{-1} \sum_q S_q e^{i\Omega_q \tau} \right] \exp\left[N^{-1} \sum_q S_q e^{-i\Omega_q \tau'} \right] \exp\left[N^{-1} \sum_q S_q e^{-iq\cdot\Delta} e^{i\Omega_q \sigma} (e^{i\Omega_q \tau} - 1)(e^{-i\Omega_q \tau'} - 1) \right], \quad (3.22)$$

$$\Delta \equiv l - l'. \quad (3.23)$$

Let us consider the significance of the summation over Δ in Eq. (3.22). The symbols l and l' denote the sites from which the secondary photon is radiated. Therefore, terms containing Δ express the phase difference of the photon radiated from each site. Since our system is a quantum-mechanical one, we do not know in which site the core hole is created and annihilated. What we finally obtain are only the conduction electron, the valence hole, and the radiated photon, all of which are in the lattice with a translational symmetry. For this reason, we must take all possible intermediate states into account as well as the mutual interference among them. This interference effect is taken into account by the summation over Δ, and determines the spectral shape of this secondary radiation.

Expanding the last line of Eq. (3.22) with respect to S_q, and executing the integration over σ of the first line, we obtain a multiphonon expansion form for $R(\omega_1,\omega_2)$ as

$$R(\omega_1,\omega_2)\equiv|M_{vc}(k_2)M_{ac}(k_1)|^2\sum_{\nu=0}^{\infty}R_\nu(\omega_1,\omega_2), \tag{3.24}$$

$$R_0(\omega_1,\omega_2)=\frac{1}{N^3}\sum_{K,k}\sum_{\Delta}e^{i(k_1-k_2-K)\cdot\Delta}\left|\sum_{\mu=0}^{\infty}\frac{e^{-S}S^\mu}{\mu!}\int_{-\infty}^{\infty}d\Omega' D_\mu(\Omega')\int_0^\infty d\tau e^{i[\varepsilon_a(k)+\varepsilon_c-W+\Omega'-\omega_1]\tau}\right|^2$$
$$\times\delta[\varepsilon_a(k)+\varepsilon_v(K-k)+\omega_2-\omega_1], \tag{3.25}$$

$$R_\nu(\omega_1,\omega_2)=\frac{1}{N^3}\frac{1}{\nu!}\sum_{q_1,\ldots,q_\nu}\left(N^{-\nu}\prod_{i=1}^{\nu}S_{q_i}\right)\sum_{K,k}\sum_{\Delta}e^{i\left(k_1-k_2-K-\sum_{i=1}^{\nu}q_i\right)\cdot\Delta}\left|\sum_{\mu=0}^{\infty}\frac{e^{-S}S^\mu}{\mu!}\int_{-\infty}^{\infty}d\Omega' D_\mu(\Omega')\right.$$
$$\left.\times\int_0^\infty d\tau e^{i[\varepsilon_a(k)+\varepsilon_c-W+\Omega'-\omega_1]\tau}\left[\prod_{i=1}^{\nu}(e^{i\Omega_{q_i}\tau}-1)\right]\right|^2\delta\left[\varepsilon_a(k)+\varepsilon_v(K-k)+\sum_{i=1}^{\nu}\Omega_{q_i}+\omega_2-\omega_1\right]\quad(\nu=1,2,\ldots), \tag{3.26}$$

where R_ν denotes a rate of the transition process which lefts ν phonons in the final state, as well as the conduction electron, the valence hole, and the photon. Here we have introduced a μ-fold phonon density function $D_\mu(\Omega)$ as

$$D_\mu(\Omega)\equiv\int_{-\infty}^{\infty}d\Omega_1'\cdots\int_{-\infty}^{\infty}d\Omega_\mu'\left[\prod_{i=1}^{\mu}D(\Omega_i')\right]$$
$$\times\delta\left(\Omega-\sum_{i=1}^{\mu}\Omega_i'\right)\quad(\mu=1,2,\ldots), \tag{3.27}$$

$$D(\Omega)\equiv\frac{1}{SN}\sum_q S_q\delta(\Omega-\Omega_q), \tag{3.28}$$

$$D_0(\Omega)\equiv\delta(\Omega). \tag{3.29}$$

The wave vectors of the incident and the radiated photon k_1 and k_2 are sufficiently small compared with that of electrons and phonons. Therefore, we can approximate $k_1=k_2=0$, hereafter. We also introduce the energy width $(2\gamma_R)$ of the core hole, and this width includes all the decay processes of the core hole such as the radiative decay and the Auger decay, phenomenologically. This γ_R does not include all the possible decay processes of the excited state. For example, nonradiative decay processes of the conduction electron are omitted. After taking the summation over Δ in Eqs. (3.25) and (3.26), and using this γ_R, we finally obtain

$$R_0(\omega_1,\omega_2)=\frac{1}{N}\sum_k\left|\sum_{\mu=0}^{\infty}\frac{e^{-S}S^\mu}{\mu!}\int_{-\infty}^{\infty}d\Omega' D_\mu(\Omega')\int_0^\infty d\tau e^{i[\varepsilon_a(k)+\varepsilon_c-W+\Omega'-\omega_1+i\gamma_R]\tau}\right|^2\delta[\varepsilon_a(k)+\varepsilon_v(-k)+\omega_2-\omega_1], \tag{3.30}$$

$$R_\nu(\omega_1,\omega_2)=\frac{1}{N^{2+\nu}\nu!}\sum_{q_1,\ldots,q_\nu}\left(\prod_{i=1}^{\nu}S_{q_i}\right)\sum_{K,k}\delta\left(K+\sum_{i=1}^{\nu}q_i\right)$$
$$\times\left|\sum_{\mu=0}^{\infty}\frac{e^{-S}S^\mu}{\mu!}\int_{-\infty}^{\infty}d\Omega' D_\mu(\Omega')\int_0^\infty d\tau\, e^{i[\varepsilon_a(k)+\varepsilon_c-W+\Omega'-\omega_1+i\gamma_R]\tau}\left[\prod_{i=1}^{\nu}(e^{i\Omega_{q_i}\tau}-1)\right]\right|^2$$
$$\times\delta\left[\varepsilon_a(k)+\varepsilon_v(K-k)+\sum_{i=1}^{\nu}\Omega_{q_i}+\omega_2-\omega_1\right]. \tag{3.31}$$

Here R_0 denotes the rate of the no-phonon process. Once ω_1 is given, as schematically shown in Fig. 1, the momenta of the core hole and the conduction electron are determined by the resonant condition $[\varepsilon_a(k)+\varepsilon_c-\omega_1]\simeq 0$. This condition comes from the integral over τ in Eq. (3.30). Therefore, the valence electron which can go down to the core band is also uniquely determined. Consequently, ω_2 itself is also determined by the δ function in Eq. (3.30). This process does not contain the dissipation of the core-hole momentum at all, while R_ν denotes the rate of the ν-phonon process. In the first line of Eq. (3.31), we have a δ function which is absent in the case of Eq. (3.30). It implies the total momentum conservation, and means that the momentum of the core hole, determined by the aforementioned resonance condition, dissipates throughout the solid by the ν phonons. For these reasons, the competition between the dissipation time of the phonons and the lifetime of the core hole play an important role in the spectral shape of the radiated photon.

One may ask why the core hole, which is well localized within each atomic core, can have such a definite momentum. The answer is as follows. Since the core hole at each site is created by the same photon, the phase relation among the sites is well defined by the aforementioned resonant condition. In this situation it can be regarded that the core hole has a definite momentum. When the core hole disappears, a new photon will be radiated. However, the new photon inherits this phase relation faithfully, and results in self-interference as explained before in connection with Eqs. (3.22) and (3.23). If this photon is radiated before the core-hole momentum dissipates, the rate of this process is denoted mainly by R_0. Therefore, in this case, the spectrum of the radiated photon mainly contributes to the Raman component, and shows a sharp peak unlike the DOS, as shown in Fig. 1. If the photon is radiated after the dissipation is completed, however, the rate is mainly denoted by $\Sigma_{\nu=1}^{\infty}R_\nu$. In this case, the core hole is almost equally distributed throughout the momentum space.

If we change our viewpoint from momentum space to real space, we can understand that a phonon wave packet is generated at a certain site, propagates to other sites, and dissipates throughout the solid. Thus the energy of the core hole in this site decreases, as shown in Eq. (3.21). Therefore, the phase relation mentioned above disappears. Even in this case, this energy lowering (W) of the core hole is very difficult to observe, since it is sufficiently smaller than that of the x ray. A valence electron with any momentum is now ready to go down to the core band, since the aforementioned phase relation has disappeared. Consequently, the spectrum fully reflects the DOS, and results in the luminescence shown in Fig. 1. The above-mentioned points are the essential concepts of the resonant second-order optical process in the core-hole region, and are clarified by our theory for the first time, to our knowledge. We should note that this situation is entirely different from the case of the photoelectron emission by the soft-x-ray excitation of the core electron. In this case, the excitations started from each site are completely orthogonal, and cannot interfere each with other, since a core hole created at a certain site survives even in the final state. In Sec. IV, we will present our numerical results for the transition rate.

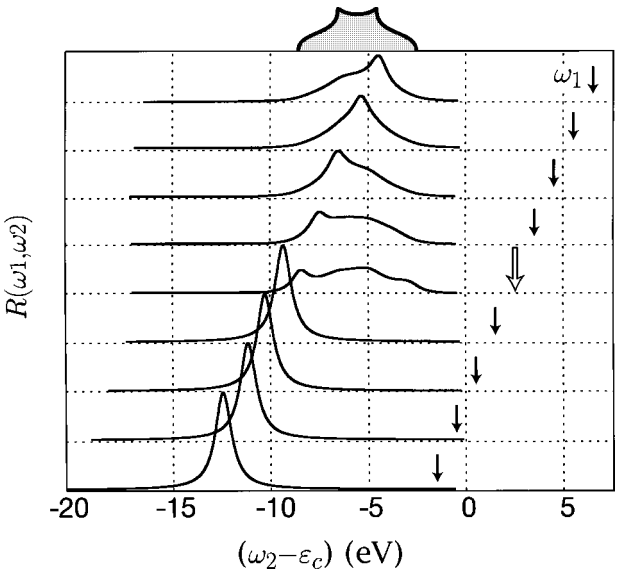

FIG. 2. $R(\omega_1,\omega_2)$ as a function of ω_1 and ω_2, of the indirect gap. $\varepsilon_g=5$ eV, $T_a=0.5$ eV, $T_v=0.5$ eV, and $2\gamma_R=0.01$ eV. The arrow indicates ω_1. The specially outlined arrow is the beginning of the resonance. Each spectrum is normalized so that its integrated intensity is unity. The shaded curve is the DOS.

IV. NUMERICAL RESULTS

For practical calculations, as mentioned above, we use two types of band gaps: indirect and direct. As we will show below, this difference is very important. Cubic BN has an indirect band gap, and hexagonal BN a direct band gap. As a typical example for both cases, ε_g, T_v, and T_a are set at 5, 0.5, and 0.5 eV, respectively. The transition dipole matrix elements $M_{ac}(k_1)$ and $M_{vc}(k_2)$ are approximated to be independent of the wave vectors of photons. As for the phonon dispersion, Ω and γ are set at 0.08 and 0.0233 eV, as a typical example. S_q is assumed to be independent of q, and is set at 1.5, as an example of weak coupling. Due to this small S_q, numerical calculations for $R(\omega_1,\omega_2)$ in Eqs. (3.24), (3.30), and (3.31) can be terminated up to $\mu=3$ and $\nu=2$.

A. Indirect-gap case

Figures 2–4 show the spectra of the indirect-gap cases. Each curve is normalized so that its integrated intensity is unity. Hereafter, we denote the dissipation time of a phonon by τ_p, and the lifetime of the core hole by τ_R. In terms of γ and γ_R, these are given as $\tau_p=(6\gamma)^{-1}$ and $\tau_R=(2\gamma_R)^{-1}$. In Fig. 2, the spectra are calculated by setting $2\gamma_R=0.01$ eV, that is, τ_p is shorter than τ_R. In this figure, arrows indicate the incident x-ray energy, and the specially outlined large arrow indicates the energy of resonance with the conduction-band edge. Spectra of the low-energy off-resonance case have a sharp peak centered at ω_1-11 eV. The reason of such profile is as follows. The spectrum of this case is composed only of the Raman component, because the x ray is radiated through the virtual processes. Furthermore, the total rate of this process is composed almost of R_0, because other rates ($R_\nu,\nu=1,2,\ldots$) are for higher-order perturbation processes. For these reasons, the spectrum shows a joint density

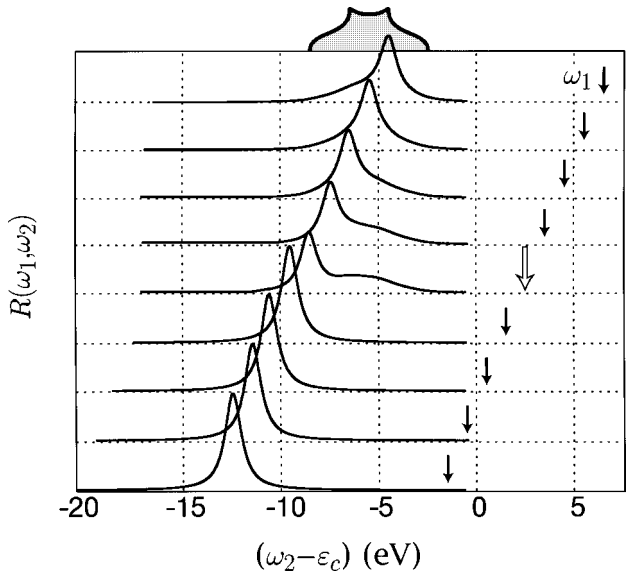

FIG. 3. Same as Fig. 2, but with $2\gamma_R=0.06$ eV.

of states between the conduction electron and the valence hole under the condition that their total wave vector K, defined in connection with Eq. (2.11), is zero. In the case of the present band structure, the energy difference between conduction and valence bands with the same wave vector is always 11 eV. Therefore, the total energy of the electron-hole pair left at the final state is always 11 eV, too. This situation is schematically shown in Fig. 5. On the other hand, spectra of the resonance, shown in Fig. 2, are composed of a small Raman component and a large luminescence component which fully reflects the DOS. The Raman component moves across the luminescence component from the low-energy to high-energy side as the incident energy increases, just as shown in Fig. 2.

Let us turn to Fig. 3. In this case, the spectra are calculated by setting $2\gamma_R=0.06$ eV, that is, τ_R and τ_p are almost comparable. In the case of resonance, the intensity of the luminescence component becomes comparable to that of the Raman component. In the case of Fig. 4, the spectra are

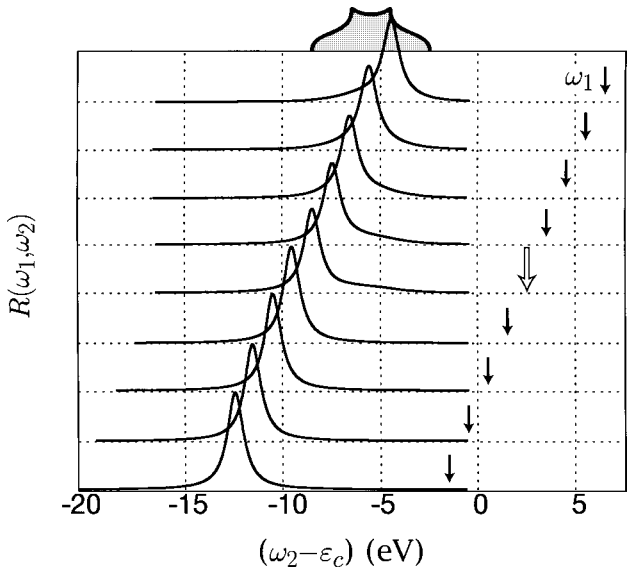

FIG. 4. Same as Fig. 2, but with $2\gamma_R=0.2$ eV.

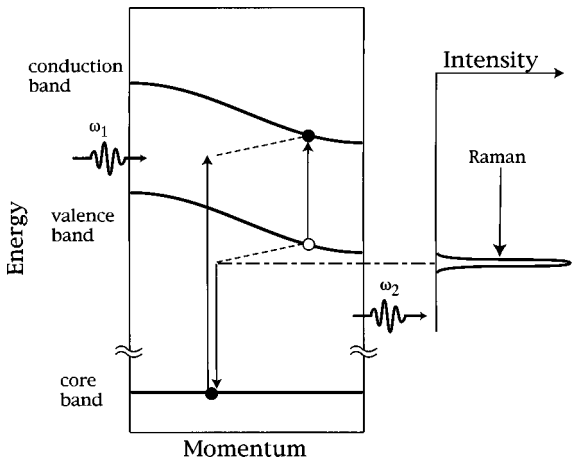

FIG. 5. Schematic diagram of the low-energy off-resonance of the indirect gap (left portion). The spectrum of the x-ray radiation (right portion).

calculated by setting $2\gamma_R=0.2$ eV, and hence, τ_p is longer than τ_R. Even in the resonance cases, we can see that the intensity of the luminescence component becomes much smaller than that of the Raman component.

Let us now show a relation among τ_p, τ_R, and the spectral shape, qualitatively. As shown in Fig. 1, the excited state created by the incident x ray has two decay channels. One is a radiative decay channel and the other is the dissipation channel by the phonons. The total decay rate is $(\tau_R^{-1}+\tau_p^{-1})$, and a partial intensity for the dissipation channel is $\tau_p^{-1}/(\tau_R^{-1}+\tau_p^{-1})$. The rest becomes $\tau_R^{-1}/(\tau_R^{-1}+\tau_p^{-1})$, and this is nothing but a partial intensity for the radiative decay channel. The former partial intensity is equal to the luminescence component, and the rest is the Raman one. Thus the Raman component becomes dominant, as τ_R becomes shorter. Our calculated results are consistent with this theorem. Let us finally mention the S_q dependence of the spectra. Even if τ_p is shorter than τ_R, the Raman component becomes dominant as S_q decreases from 1.5 to 0.

B. Direct-gap case

Figures 6–8 show the spectra of the direct-gap cases. In Fig. 6, the spectra are calculated by setting $2\gamma_R=0.01$ eV, and hence, τ_p is shorter than τ_R. Spectra of the low-energy off-resonance case are broadened and range from ω_1-17 eV to ω_1-5 eV. The reason of such profile is as follows. The energy difference between conduction and valence bands with the same wave vector is distributed from 5 to 17 eV, unlike the indirect-gap case. Therefore, a total energy of the electron-hole pair left at the final state also ranges from 5 to 17 eV. Thus the spectra have a broad profile, and this situation is shown schematically in Fig. 9. In the resonance cases, shown in upper curves of Fig. 6, spectra are composed of the small Raman and the large luminescence components, which also fully reflects the DOS. The Raman component moves across the luminescence from the high- to low-energy side, as the incident energy increases, contrary to the aforementioned indirect cases. This type of behavior of the Raman

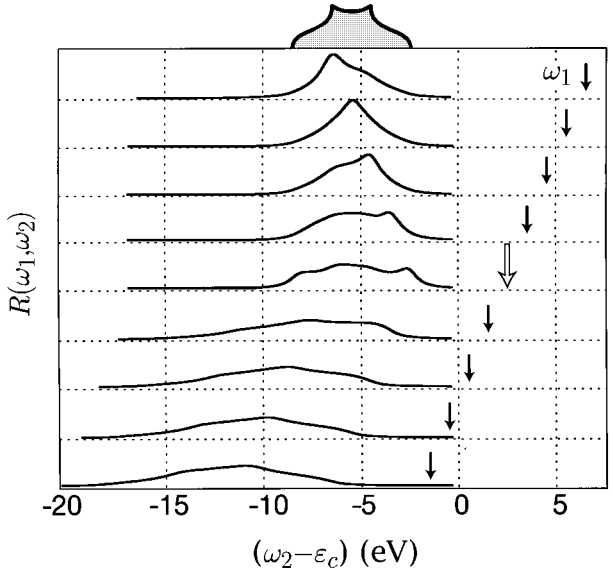

FIG. 6. The spectra in the case of the direct gap with $2\gamma_R = 0.01$ eV.

component was reported by Carlisle *et al.* [10] in their experiment on the C $1s \leftrightarrow 2p$ transitions of graphite.

As τ_R becomes short relative to τ_p, the Raman component becomes dominant in the spectra, as shown in Figs. 7 and 8. However, the S_q dependence of these spectra are same as the indirect cases.

Let us now turn to the nature of the total integrated intensity $I(\omega_1)$, which is defined as

$$I(\omega_1) \equiv \int_{-\infty}^{\infty} d\omega_2 R(\omega_1,\omega_2). \tag{4.1}$$

Figure 10 shows $I(\omega_1)$ as a function of ω_1. This result shows $I(\omega_1)$ suddenly increase as the resonance condition is satisfied.

It should be noted that, in such an off-resonance region of ω_1,

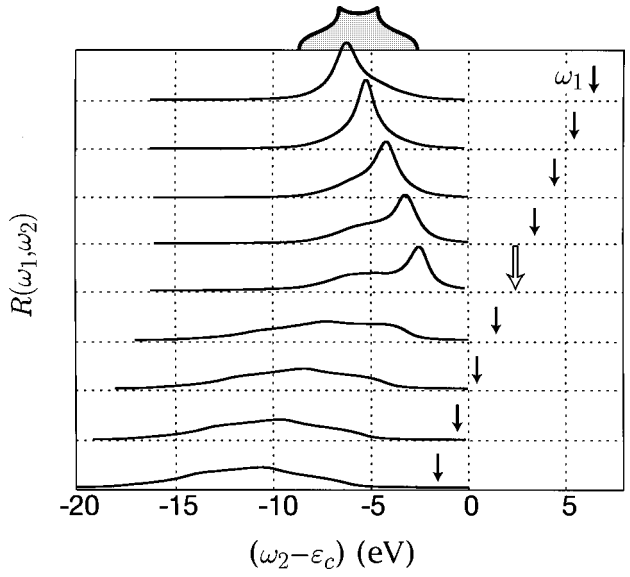

FIG. 7. Same as Fig. 6, but with $2\gamma_R = 0.06$ eV.

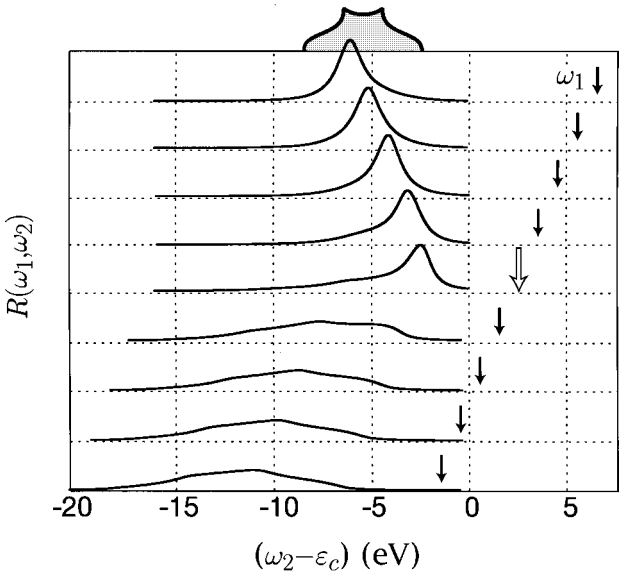

FIG. 8. Same as Fig. 6, but with $2\gamma_R = 0.2$ eV.

$$|\varepsilon_g/2+\varepsilon_c-\omega_1| \gg \gamma_R, W, \Omega',$$

$I(\omega_1)$, given from Eqs. (3.30), (3.31), and (4.1), simply becomes

$$I(\omega_1) \propto \frac{1}{(\varepsilon_g/2+\varepsilon_c-\omega_1)^2}.$$

Therefore, its behavior is almost independent of γ_R, and is also common to both direct and indirect cases.

V. CONCLUSION AND DISCUSSION

So far, we have clarified the dynamics of the core-hole momentum dissipation due to phonons in the soft-x-ray radiation processes from the valence band to the core level. We have also clarified how the DOS of the valence band is reflected in the SXRS spectra, and why these spectra separate into Raman and luminescence components.

The spectra of the low-energy off-resonance case are composed only of the Raman component. They reflect the joint density of states of the conduction and valence bands under the condition that the total momentum (K) of the electron-hole pair left at the final state is zero. We cannot obtain sufficient information about the DOS from the spectra of the low-energy off-resonance case. In the resonance case, on the other hand, the spectra are composed of Raman and luminescence components. Only the latter fully reflects the DOS.

The intensity ratios between the two components, i.e., the luminescence and Raman, are determined by three factors: the dissipation time (τ_p) of a phonon, the lifetime (τ_R) of the core hole, and the strength (S) of the core-hole–phonon interaction. We can obtain various cases, i.e., the Raman-dominant case, the luminescence-dominant case, and the intermediate cases. When τ_R is shorter than τ_p, the intensity of the Raman component becomes greater than that of the luminescence component. However, if τ_R and τ_p are comparable, the intensity of the Raman component becomes comparable with that of the luminescence component. On the

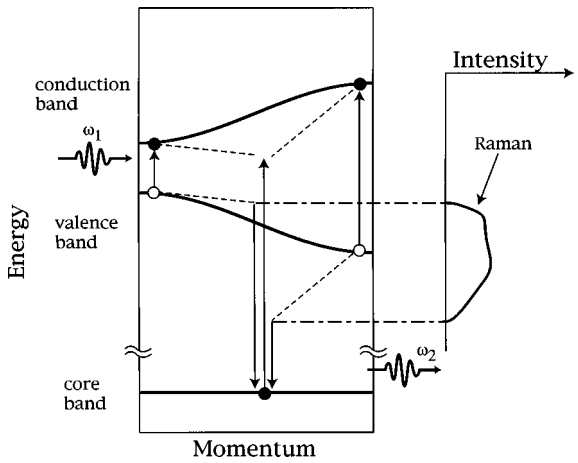

FIG. 9. Schematic diagram of the low-energy off-resonance of the direct gap (left portion). The spectrum of the x-ray radiation-(right portion).

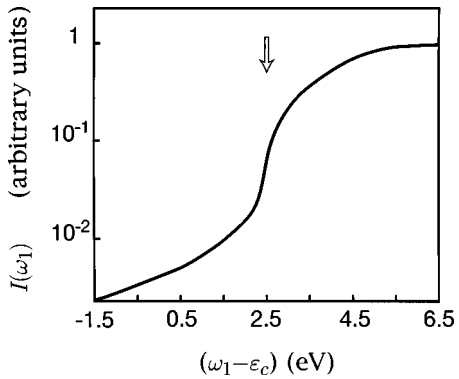

FIG. 10. $I(\omega_1)$ as a function of ω_1. The outlined arrow is the beginning of the resonance.

other hand, if τ_R is longer than τ_p, the intensity of the luminescence component becomes higher than that of the Raman components. Thus we can obtain various situations. The Raman-dominant situation seems to be realized in the Mn $2p \leftrightarrow 3d$ transitions of MnO reported in Ref. 5. The intermediate situation is realized in the Ti $2p \leftrightarrow 3d$ transition of TiO_2 reported in Ref. 3, and also in the Ca $2p \leftrightarrow 3d$ transition of CaSi and $CaSi_2$ reported in Ref. 4. On the other hand, the luminescence-dominant situation is realized in the B $1s \leftrightarrow 2p$ transition of cubic BN reported in Ref. 1, and the hexagonal BN transition reported in Ref. 2. Additionally, the behavior of the Raman component in the direct-gap cases is realized in the C $1s \leftrightarrow 2p$ transition of graphite reported in Ref. 10.

Let us discuss the broken symmetry of the translational invariance of the lattice, due to a creation of the core hole. If we have a core hole in a certain cite (l), this state is completely orthogonal to a state with a core hole in another site (l'). In this case, we have a well-defined broken symmetry. In our second-order optical process, however, the core hole is created and subsequently annihilated, and what we finally obtain are a conduction electron, a valence hole and a radiated photon, all of which are in the lattice. Consequently, the translational symmetry is recovered at the final state.

Let us now consider differences between the resonant second-order optical process in the x-ray region and that of the visible region. The optical process which we discussed in this paper is essentially the same as that of the visible region.[11] However, in the visible region, the radiative lifetime of the intermediate state is about 10^{-9} s. Since this lifetime is much longer than the dissipation time of the phonon, the intensity of the luminescence is usually much stronger than that of the resonant Raman scattering. For this reason, the competition between τ_R and τ_p is a distinctive feature which appears most typically in the present soft-x-ray region.

Finally, the following problems are left unsolved, and are targets of our future studies: core exciton effects, [12] valence exciton effects, cases with strong S, many-band (more than three) cases, and multielectron excitation effects. To study mechanisms determining an intensity ratio between Rayleigh and Raman scattering is also a problem to be dealt with in our future work.

ACKNOWLEDGMENTS

The authors are much obliged to Professor S. Shin and Dr. A. Agui for providing valuable information on this experimental study before publication.

[1] A. Agui, S. Shin, M. Fujisawa, Y. Tezuka, T. Ishii, Y. Muramatsu, O. Mishima, and K. Era, Phys. Rev. B **55**, 2073 (1997); A. Agui, S. Shin, M. Fujisawa, Y. Tezuka, T. Ishii, O. Mishima, K. Era, E. Shigemasa, and A. Yagishita, J. Electron Spectrosc. Relat. Phenom. **79**, 191 (1996).

[2] J. J. Jia, T. A. Callcott, Eric L. Shirley, J. A. Carlisle, L. J. Terminello, A. Asfaw, D. L. Ederer, F. J. Himpsel, and R. C. C. Perera, Phys. Rev. Lett. **76**, 4054 (1996).

[3] Y. Tezuka, S. Shin, A. Agui, M. Fujisawa, and T. Ishii, J. Phys. Soc. Jpn. **65**, 312 (1996); Y. Tezuka, S. Shin, A. Agui, M. Fujisawa, T. Ishii, and A. Yagishita, J. Electron Spectrosc. Relat. Phenom. **79**, 195 (1996).

[4] J. J. Jia, T. A. Callcott, A. Asfaw, J. A. Carlisle, L. J. Terminello, D. L. Ederer, F. J. Himpsel, and R. C. C. Perera, Phys. Rev. B **52**, 4904 (1995); R. C. C. Perera, J. J. Jia, T. A. Callcott, J. A. Carlisle, L. T. Terminello, F. J. Himpsel, and D. L. Ederer, J. Electron Spectrosc. Relat. Phenom. **79**, 139 (1996).

[5] S. M. Butorin, J.-H. Guo, M. Magnuson, P. Kuiper, and J. Nordgren, Phys. Rev. B **54**, 4405 (1996).

[6] A. Agui, Ph.D. thesis, The University of Tokyo, 1996.

[7] Y. Ma, P. Skytt, N. Wassdahl, P. Glans, D. C. Mancini, J. Guo, and J. Nordgren, Phys. Rev. Lett. **71**, 3725 (1993).

[8] Y. Toyozawa, A. Kotani, and A. Sumi, J. Phys. Soc. Jpn. **42**, 1495 (1977).

[9] R. Kubo, J. Phys. Soc. Jpn. **17**, 1100 (1962).

[10] J. A. Carlisle, L. J. Terminello, J. J. Jia, T. A. Callcott, D. L. Ederer, R. C. C. Perera, and F. J. Himpsel, in *Proceedings of the Workshop Raman Emission by X-ray Scattering, New Orleans 1995*, edited by D. L. Ederer and J. H. McGuire (World Scientific, Singapore, 1996), p. 41.

[11] Y. Toyozawa, J. Phys. Soc. Jpn. **41**, 400 (1976).

[12] M. van Veenendaal and P. Carra, Phys. Rev. Lett. **78**, 2839 (1997).